Wang, J. & Gutierrez, M. (2010). *Géotechnique* **60**, No. 5, 395–409 [**doi:** 10.1680/geot.2010.60.5.395]

Discrete element simulations of direct shear specimen scale effects

J. WANG* and M. GUTIERREZ†

This paper presents a study of the micromechanics of granular materials as affected by the direct shear test scale using the discrete element method (DEM). Parametric studies were conducted to investigate the effects of specimen length and height scales (in relation to the particle size) on the bulk material shear strength and shear banding behaviour in the direct shear test. A mesh-free strain calculation method previously developed by the authors was used to capture and visualise the evolution of strain localisation inside the direct shear box. Simulation results show that the maximum shear strength measured at the model boundaries increases with decreasing specimen length scale and increasing specimen height scale. Micromechanics-based analysis indicates that the local and global aspects of fabric change and failure are the major mechanisms responsible for the specimen scale effect. Global failure along the primary shear band prevails when the specimen length scale and length to height aspect ratio are small, while progressive failure becomes more likely when the specimen length scale and aspect ratio become larger. Further quantifications of the specimen scale effects on the macroscopic behaviour of granular materials rely on the fundamental understanding of quantitative relationships between material fabric, anisotropy and bulk strength.

KEYWORDS: fabric/structure of soils; failure; numerical modelling; shear strength; strain localisation

La présente communication présente une étude de la micromécanique de matières granulaires affectées par l'échelle d'essais de cisaillement direct faisant usage de la DEM (méthode aux éléments discrets). On a effectué des études paramétriques pour examiner les effets d'échelles spécimen de longueur et de hauteur (en fonction de la granulométrie) sur la résistance au cisaillement des matières en vrac et le comportement de rubannement au cisaillement dans les essais de cisaillement directs. On a utilisé une méthode de calcul des déformations non maillée, créée précédemment par les auteurs, pour saisir et visualiser l'évolution de la localisation des déformations à l'intérieur de la boîte d'essai de cisaillement direct. Les résultats de la simulation indiquent que la longueur de cisaillement maximale, mesurée aux limites du modèle, augmente au fur et à mesure de la diminution de l'échelle de longueur du spécimen et de l'augmentation de son échelle de hauteur. L'analyse à base de micromécanique indique que les aspects locaux et globaux de variation et de rupture de l'enveloppe sont les principaux mécanismes qui déterminent l'effet d'échelle du spécimen. La rupture globale le long du ruban de cisaillement primaire est prévalente lorsque l'échelle de longueur et le ratio de l'aspect longueur /hauteur sont limités, tandis que la rupture progressive devient plus probable lors de l'augmentation de l'échelle de longueur et du ratio de l'aspect. Certaines quantifications supplémentaires des effets d'échelle du spécimen sur le comportement macroscopique de matières granulaires sont tributaires de connaissances fondamentales sur les rapports quantitatifs entre l'enveloppe, l'anisotropie, et la résistance de volume.

INTRODUCTION

Specimen scale effects in the direct shear apparatus (DSA) on the shear strength parameters of granular soils has been a well-studied topic since the 1930s, when Parsons (1936) showed the variation of sand friction angle as a function of the shear box size. The nature of the problem lies in the artificial boundary effects introduced by the shear box boundaries on the deformation and strength behaviour of soils. When the shear box apparatus does not correctly simulate the actual field conditions under which the soil deforms, doubt is cast upon the reliability of test results to be used in practical engineering designs. Besides the specimen scale effects, other testing-related issues of the DSA include non-uniform stress and strain, and the associated progressive failure inside the specimen (Terzaghi & Peck, 1948; Hvorslev, 1960; Saada & Townsend, 1981). In addition, ambiguities exist in interpreting shear strength parameters owing to the fact that principal stress rotation occurs continuously until the peak state, and the failure plane may deviate from the horizontal mid-plane (Morgenstern & Tchalenko, 1967; Jewell & Wroth, 1987).

In spite of these problems, the direct shear testing remains popular owing to its simplicity and lower testing cost than other sophisticated tests. Furthermore, standard test procedures (ASTM D5321-02) (ASTM, 2002) to determine the frictional strength of geosynthetic–soil interfaces are based on the direct shear test. For these reasons, more experimental and numerical studies on the test have been conducted in the past three decades (Arthur *et al.*, 1977; Scarpelli & Wood, 1982; Jewell & Wroth, 1987; Potts *et al.*, 1987; Palmeira & Milligan, 1989; Alshibli & Sture, 2000; Lings & Dietz, 2004; Cerato & Lutenegger, 2006; Wang *et al.*, 2007b). Some major conclusions of these studies include: (*a*) stresses and strains within the final failure zone are fairly uniform and progressive failure effects are minor, despite the non-uniform stresses and strains imposed by the box (Jewell & Wroth, 1987; Potts *et al.*, 1987); (*b*) the peak shear strength from DSA is very close to that obtained in an ideal simple shear condition, and the deviation of the zero linear extension direction at peak from the horizontal is negligible (Potts *et al.*, 1987; Wang *et al.*, 2007b); (*c*) multiple shear bands propagate from the edge of the box towards the middle of the specimen, appearing as a function of specimen

Manuscript received 4 January 2009; revised manuscript accepted 8 October 2009.
Discussion on this paper closes on 1 October 2010, for further details see p. ii.
* Department of Building and Construction, City University of Hong Kong, Hong Kong.
† Division of Engineering, Colorado School of Mines, Golden, CO 80401, USA.

length, height and soil density (Scarpelli & Wood, 1982; Wang *et al.*, 2007b); (*d*) the measured friction angle generally decreases with increasing box size above a certain box size to maximum particle diameter ratio, owing to the room available in the box for the shear zone to develop fully (Jewell & Wroth, 1987; Cerato & Lutenegger, 2006). These findings largely clarify the aforementioned controversial issues existing in the history of the use of DSA and provide strong justification for the validity of DSA peak state data as compared with the simple shear testing. For geotechnical engineers and practitioners, these studies provide useful insights in the understanding and interpretation of direct shear test results.

With the above brief review of the literature on direct shear testing, this paper re-examines the problem of DSA scale effects. This topic has been the focus of many studies but is still not fully understood. Two important interwoven issues involved in this topic are: (*a*) the effects of box size (i.e. box length and box height in relation to the maximum/median particle diameter) on the macroscopic shear stress ratio (or peak friction angle); and (*b*) the effects of box size on the extent of localised shear zone developed inside the box. The first issue is critical to the goal of the research, which is to determine and recommend an appropriate DSA size that could yield the true shear strength parameters of a soil, whereas the second issue essentially concerns the mechanism responsible for the observed scale effects.

ASTM D 3080-90 (ASTM, 1990) requires a minimum specimen thickness of six times the maximum particle diameter and a minimum specimen length of 10 times the maximum particle diameter. However, experimental and numerical evidences presented in the literature show that the current ASTM D 3080-90 criteria may not provide the true soil friction angle because the specified sizes could still impede the full growth and propagation of the shear band inside the specimen. Parsons (1936) showed that the friction angle of a crushed quartz and a clean uniform sand decreases slightly with the increasing box size under low normal stresses. Using radiographs, Scarpelli & Wood (1982) found that the shear band thickness varied along the length of the shear zone and reached a maximum value around $10D_{50}$ during steady state. They concluded that the particular bifurcation followed by the sand depended on the degree of constraint imposed on the sand, and suggested a value of $100D_{50}$ for box length in order to allow for the full propagation of the shear band. Palmeira & Milligan (1989) performed tests on dense Leighton Buzzard 14/25 sand ($D_{50} = 0{\cdot}8$ mm and $D_r = 87\%$) using shear box length and height varying from $40D_{50}$ to $1250D_{50}$, and $75D_{50}$ to $1250D_{50}$ respectively. They found little change of the measured friction angle but large variation of the shear zone thickness with the scale of the test. A complete review of the literature on the influence of box size and scale on the shear zone thickness was given by Cerato & Lutenegger (2006). They also showed experimental test data on five sands with varying densities, which demonstrate the considerable effects of box size on the constant volume friction angle and suggested the use of at least $50D_{max}$ for the box length or width. Recently, Jacobson *et al.* (2007) performed discrete element simulations of direct shear test on uniform specimens and showed that the well-defined shear zone only developed when the specimen-to-particle size ratio was not less than 58. Zhang & Thornton (2007) also performed a detailed two-dimensional (2D) discrete element method (DEM) study of the direct shear test and concluded that the evolution of stress ratio inside the shear zone is not significantly affected by the aspect ratio, but the difference between the stress ratio measured in the shear zone and that calculated from the boundary forces reduces if the aspect ratio is reduced. This conclusion, however, was only based on limited parametric studies of the aspect ratio, and did not provide the micromechanical mechanisms of the aspect ratio effects, which is the major thrust of the current paper. The preliminary 2D DEM study by Wang & Gutierrez (2009) proposed the grain-scale mechanism of DSA length scale effects, which essentially is controlled by the specimen aspect ratio. Further details of micromechanical evidences and analyses supporting the proposed mechanism are not given in that study.

This paper presents a comprehensive study of the DSA scale effect using DEM, which is a highly valuable but underutilised tool for exploring the micromechanics of granular soils subjected to external loading. Two-dimensional DEM simulations of the direct shear box test filled with rigid spherical particles of uniform or varying sizes are performed using PFC2D (Particle Flow Code 2D) developed by Itasca Consulting Group, Inc. (2002). Variables including box length (L) and height (H), specimen gradation (D_{max}/D_{min}), initial specimen porosity (p_0) and normal stress (P_n) are considered in the parametric study so that the specimen scale effects can be captured for different specimen configurations. Macroscopic model behaviour is interpreted using the stress and volume change data of bulk material measured at the boundaries. Furthermore, using the strain calculation method previously developed by the authors (Wang *et al.*, 2007a; 2007b), the shear zone developed inside the specimen as a function of the above variables is visualised and analysed. The micromechanics-based shear banding analysis is used to provide fundamental explanation of the effects that the model test scale has on the discrete continuum scale behaviour of granular soils inside the DSA.

DEM SIMULATIONS

Model set-up

The DEM model of a direct shear box shown in Fig. 1 is created in an effort closely to mimic the physical DSA in the laboratory. Assemblages of rigid spherical particles with varying sizes are generated to fill the specified volume and allowed to consolidate at a particular interparticle friction coefficient to achieve a target initial porosity. For all the granular specimens used, the median particle diameter (D_{50}) is equal to 0·7 mm. The largest size of the shear box used in the current study is 88 mm (L) × 56 mm (H), with both the upper and lower half of the box equal to 28 mm. This size gives the largest ratios of box length and box height to median particle diameter of about $L/D_{50} = 126$ and $H/D_{50} = 80$. Simulation results from these dimensions have been

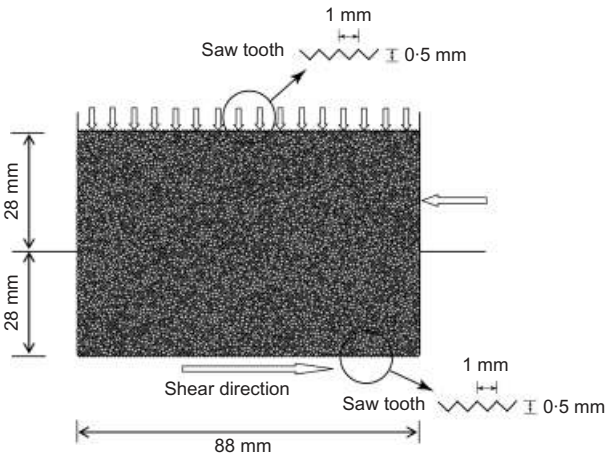

Fig. 1. DEM model of a direct shear box

validated against laboratory direct shear test results using 0·7 mm glass beads by Dove (1996) and Dove & Jarrett (2002). Glass bead properties measured in the laboratory, such as particle density, shear modulus and interparticle friction coefficient were directly used in the simulations discussed herein.

Owing to the large dimensions, the model size was found by Wang (2006) to reproduce well the direct shear behaviour of granular materials with a minimum influence of boundary interference, as will be shown later. A study on DEM simulations of direct shear test of sands using the above model was presented by Wang *et al.* (2007b). Besides choosing an appropriate model size, Wang (2006) also found through the model validation process that the particle to wall friction is an important parameter critical to the initial shear stiffness, peak friction angle and shear banding behaviour of the bulk material. A high value of 0·9 was selected for this parameter to prevent any slip between the bulk material and the boundary walls. In addition, the top and bottom boundaries were further roughened by introducing continuous 1 mm-wide sawtooth-shaped grooves (Fig. 1), as recommended by the Institution of Chemical Engineers standard (IChemE, 1989) and adopted in a recent relevant study by Hartl & Ooi (2008). These model settings are used in the current study.

Specimens are first consolidated to equilibrium under a specified normal stress applied on the top boundary through a servo-control mechanism. It is well recognised that the initial porosity and packing geometry will have considerable effects on the ensuing shear behaviour. Therefore, a uniform interparticle friction coefficient of 0·3 is used in the initial consolidation stage of all the simulations to minimise the variation of initial porosity owing to particle interlocking. Of course, different values of initial porosity can be obtained before shearing, which results from variations of normal stress level, shear box size and specimen gradation. These will be the exact subjects of the study presented in this paper. During the shearing process, the lower half of the box is displaced to the right at a constant velocity of 1 mm/min, while the upper half of the box is fixed. The top boundary is allowed to rotate freely and move in the vertical direction to maintain the constant normal stress. Horizontal stress, horizontal displacement and vertical displacement are evaluated at the boundaries.

The Hertz–Mindlin contact model was used in all the simulations. An additional particle rolling resistance model (Wang *et al.*, 2004) was also used at both particle–particle contacts and particle–boundary contacts. Physical constants used in the simulations include: glass bead density of 2650 kg/m^3; glass bead shear modulus of 29 GPa (Dove *et al.*, 2006); particle Poisson's ratio of 0·3; critical normal and shear viscous damping coefficient, both 1·0; time step of $5{\cdot}0\times10^{-5}$ s; and interparticle and particle–boundary friction coefficient during shear of 0·5 and 0·9 respectively. The values of model parameters, other than those directly measured, were obtained by fitting simulation results through laboratory data to obtain realistic macro and micromechanical model behaviour. Readers are referred to Wang (2006) for detailed information on model validation.

Parametric study

A total number of 48 simulations were made to investigate the shear box scale effects on the bulk shear strength and shear banding behaviour of granular materials under a wide range of normal stresses and initial porosities. Details of the parametric study are listed in Table 1. Two sets of granular specimens were used: poorly graded specimens with $D_{max}/D_{min} = 1{\cdot}1$, and well-graded specimens $D_{max}/D_{min} = 3{\cdot}0$. In both cases, particles have randomly generated diameters between D_{max} and D_{min} resulting in a nearly linear particle size distribution, but D_{50} remained equal to 0·7 mm, as mentioned before. For a given box size, the total number of particles (N) in a poorly graded specimen and a well-graded specimen are the same. The box length and box height spanned the ranges from 35 mm to 88 mm, and from 14 mm to 56 mm, respectively. This resulted in the ratios L/D_{max} and H/D_{max} varying from 48 to 120, and from 19 to 76 for

Table 1. Variables and their values in the parametric study

L: mm	H: mm	Poorly graded material ($D_{max}/D_{min} = 1{\cdot}1$)					Well-graded material ($D_{max}/D_{min} = 3{\cdot}0$)				
		N	L/D_{max}	H/D_{max}	P_n: kPa	P_0	N	L/D_{max}	H/D_{max}	P_n: kPa	p_0
88	56	11 239	120	76	100	0·12	11 239	84	53	100	0·118
88	56	11 239	120	76	50	0·135	11 239	84	53	50	0·139
88	56	11 239	120	76	25	0·143	11 239	84	53	25	0·154
88	56	11 239	120	76	10	0·156	11 239	84	53	10	0·162
88	28	5669	120	38	100	0·126	5669	84	27	100	0·121
88	28	5669	120	38	50	0·136	5669	84	27	50	0·147
88	28	5669	120	38	25	0·145	5669	84	27	25	0·164
88	28	5669	120	38	10	0·158	5669	84	27	10	0·176
88	14	2884	120	19	100	0·13	2884	84	13	100	0·127
88	14	2884	120	19	50	0·14	2884	84	13	50	0·152
88	14	2884	120	19	25	0·151	2884	84	13	25	0·169
88	14	2884	120	19	10	0·165	2884	84	13	10	0·179
63	28	4087	86	38	100	0·103	4087	60	27	100	0·119
63	28	4087	86	38	50	0·114	4087	60	27	50	0·134
63	28	4087	86	38	25	0·125	4087	60	27	25	0·138
63	28	4087	86	38	10	0·139	4087	60	27	10	0·148
63	14	2093	86	19	100	0·115	2093	60	13	100	0·131
63	14	2093	86	19	50	0·134	2093	60	13	50	0·145
63	14	2093	86	19	25	0·144	2093	60	13	25	0·157
63	14	2093	86	19	10	0·155	2093	60	13	10	0·157
35	14	1186	48	19	100	0·112	1186	33	13	100	0·12
35	14	1186	48	19	50	0·128	1186	33	13	50	0·136
35	14	1186	48	19	25	0·138	1186	33	13	25	0·148
35	14	1186	48	19	10	0·152	1186	33	13	10	0·158

poorly graded specimens, and varying from 33 to 84, and from 13 to 53 for well-graded specimens. The selected ranges of model sizes and scales were made wide enough so that their effects on model behaviour could be fully investigated. Within this range, the minimum aspect ratio (L/H) of the shear box is 1·57. Smaller aspect ratios are not selected in order to avoid the 'arching' effects appearing in the taller specimen. Normal stresses were chosen to vary from 10 kPa to 100 kPa, corresponding to a typical range of stress levels selected in the laboratory.

With the interparticle friction coefficient being the same for all the specimens during the consolidation phase, the initial specimen porosity (p_0) is only a function of normal stress (P_n), box size (L, H) and specimen gradation (D_{max}/D_{min}), as plotted in Fig. 2. Apparently, the following trends can be observed from Fig. 2 for p_0 with all the other variables being the same: (*a*) p_0 decreases with increasing P_n, and the variation between p_0 and P_n is more linear for well-graded specimens; (*b*) p_0 is higher for well-graded specimens; (*c*) p_0 decreases with increasing H; (*d*) p_0 decreases with decreasing L, but the effect is negligible for well-graded specimens when L is less than 63 mm. Interestingly, owing to the opposing trends in (*c*) and (*d*), the highest and lowest p_0 result from the combination of $L = 88$ mm and $H = 14$ mm, and the combination of $L = 63$ mm and $H = 28$ mm, respectively. The relevance of the size-dependent initial porosity (i.e. density) to the ensuing shear strength and shear banding behaviour will be addressed further later.

RESULTS AND DISCUSSION

DEM simulations excel in yielding both micro- and macro-scopic data of granular material, which facilitates the understanding of bulk material behaviour from a micromechanical point of view. The following paragraphs focus on presenting the simulation data from the parametric study as a function of model size, and seek to interpret the effects of model size/scale on a micromechanical basis.

Bulk direct shear simulation data

Bulk boundary-measured material data including peak direct shear stress ratios ($(\tau/\sigma)_{max}$), applied shear displacements (δ) and shear strains (ε) at peak shear stress ratios from all the simulations are listed in Table 2. The shear strain ε is calculated as the applied shear displacement normalised with respect to the box length. Volume changes indicated by the vertical displacement of the top wall and porosity change are also monitored throughout the shearing process. Peak stress ratios as a function of initial porosity, normal stress, specimen gradation, box length and box height are plotted in Fig. 3. It should be noted that for each box size combination (L and H), as indicated in Fig. 3, the applied normal stress increases monotonically from the right to the left as the resulting initial porosity decreases in the same direction. This fact has been well reflected in Fig. 2, but is also indicated in Fig. 3 to show the variations of $(\tau/\sigma)_{max}$ as a function of several variables. For a given box size, it is clear that the peak stress ratio increases with both decreasing normal stress and decreasing initial porosity. However, since an inverse relation exists between the normal stress and initial porosity, the final peak stress ratio is a result of competition between these two variables, dominated by whichever is prevailing. In addition, it can be seen that, with all the other conditions being the same, the well-graded material has a higher peak stress ratio than the poorly graded material. This is mainly because a higher degree of particle interlocking that exists in the well-graded material, requiring a larger amount of external work to rearrange the fabric so that a necessary volume change can be made to mobilise the full material shear strength.

It is difficult, however, to find a definitive relationship between the peak stress ratio and box size (L and H) from Fig. 3, although a general trend appears evident that a smaller box size yields a higher peak stress ratio. In order to show and interpret the respective effects of box length scale and box height scale on the direct shear behaviour of granular material, a careful study of both the macro- and microscopic simulation data is required.

Macroscopic effects of box size scale (L/D_{max}, H/D_{max}) and aspect ratio (L/H)

The macroscopic effects of box length scale and height scale can be clearly demonstrated when the peak stress ratio is plotted against the box length and box height alone, as shown in Figs 4 and 5, where the values of box height and box length are fixed respectively. Obviously, it is seen that the peak stress ratio increases with decreasing box length regardless of the normal stress level and specimen gradation. However, an opposite trend is found between the peak stress ratio and box height, with a few minor exceptions occurring

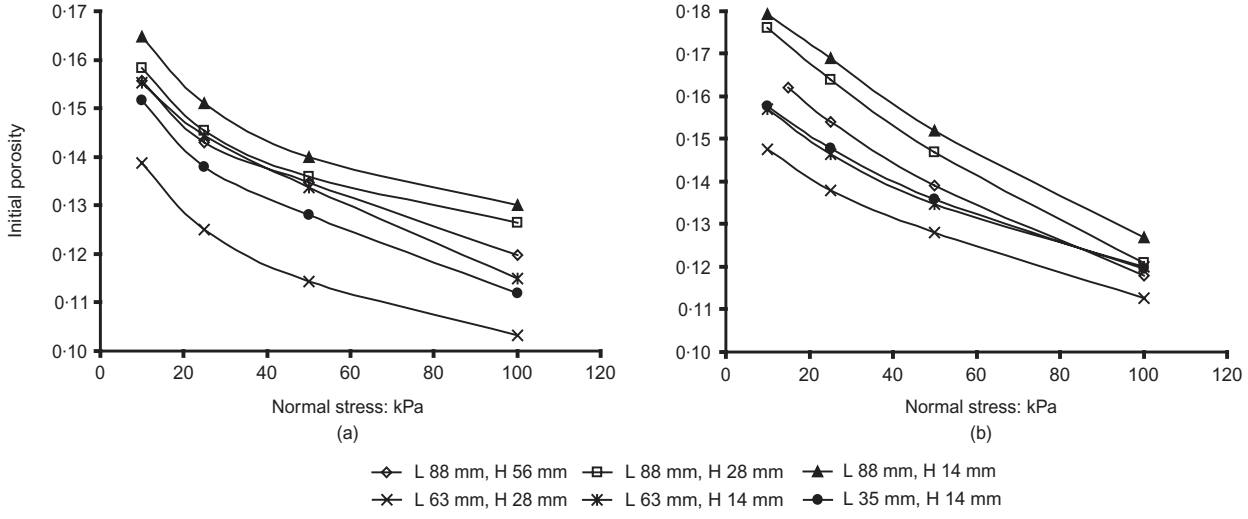

Fig. 2. Variations of initial specimen porosity (p_0) as a function of normal stress (P_n), box size (L, H) and specimen gradation (D_{max}/D_{min}): (a) poorly graded specimen; (b) well-graded specimen

Table 2. Bulk direct shear simulation data from the parametric study

				Poorly graded material ($D_{max}/D_{min} = 1{\cdot}1$)			Well-graded material ($D_{max}/D_{min} = 3{\cdot}0$)		
L: mm	H: mm	L/H	P_n: kPa	$(\tau/\sigma)_{max}$	δ^*: mm	ε^*: %	$(\tau/\sigma)_{max}$	δ^*: mm	ε^*: %
88	56	1·57	100	0·54	2·97	3·38	0·632	2·26	2·57
88	56	1·57	50	0·624	3·13	3·56	0·64	2·07	2·35
88	56	1·57	25	0·666	1·37	1·56	0·624	2·5	2·84
88	56	1·57	10	0·67	1	2·2	0·628	1·97	2·24
88	28	3·14	100	0·505	1·94	3·88	0·602	1·85	2·1
88	28	3·14	50	0·52	1·46	1·66	0·561	1·51	1·72
88	28	3·14	25	0·577	1·09	1·24	0·548	1·75	1·99
88	28	3·14	10	0·57	0·973	1·11	0·552	1·81	2·06
88	14	6·28	100	0·5	0·87	0·99	0·568	0·94	1·06
88	14	6·28	50	0·54	0·723	0·82	0·576	0·96	1·09
88	14	6·28	25	0·553	0·65	0·74	0·53	1·03	1·17
88	14	6·28	10	0·513	0·844	0·96	0·507	1·22	1·39
63	28	2·25	100	0·642	1·39	2·21	0·72	1·8	2·86
63	28	2·25	50	0·76	0·985	1·56	0·741	1·04	1·65
63	28	2·25	25	0·708	0·692	1·1	0·843	1·17	1·86
63	28	2·25	10	0·76	0·668	1·06	0·843	0·706	1·12
63	14	4·5	100	0·611	1·01	1·6	0·745	1·25	1·98
63	14	4·5	50	0·606	0·709	1·13	0·755	0·815	1·29
63	14	4·5	25	0·703	0·64	1·02	0·752	0·76	1·21
63	14	4·5	10	0·685	0·428	0·68	0·737	0·609	0·97
35	14	2·5	100	0·776	1·07	3·06	0·868	1·13	3·23
35	14	2·5	50	0·9	0·858	2·45	0·833	0·857	2·45
35	14	2·5	25	0·897	0·65	1·86	0·866	0·578	1·65
35	14	2·5	10	1·14	0·592	1·69	0·933	0·588	1·68

Note: * indicates the values of δ and ε recorded at the peak stress state, that is when $(\tau/\sigma)_{max}$ is reached

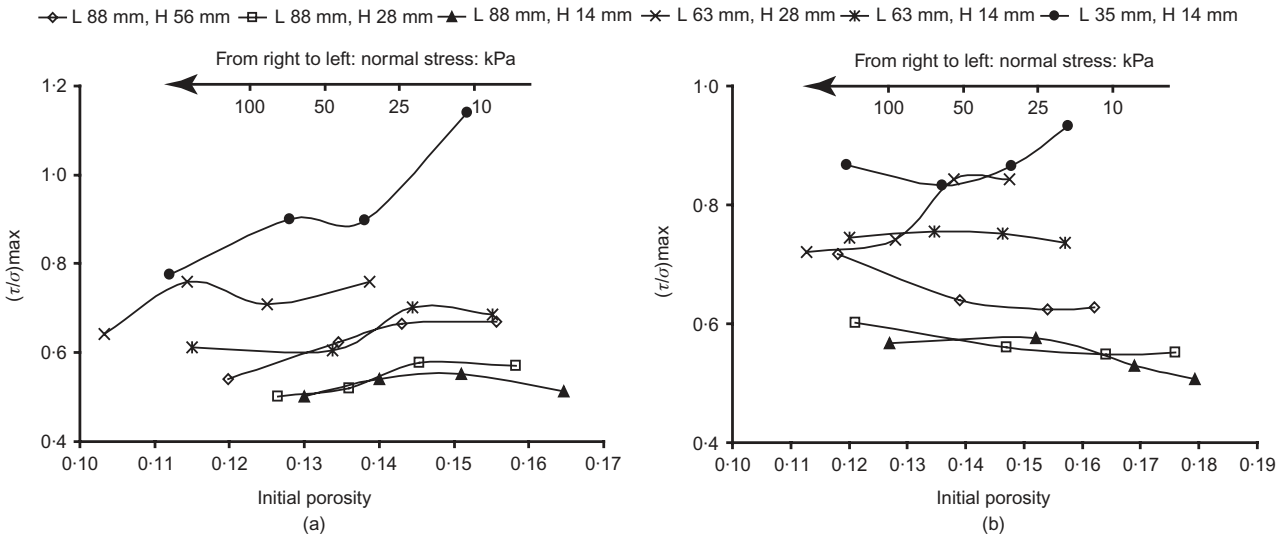

Fig. 3. Variations of peak stress ratio ($(\tau/\sigma)_{max}$) as a function of initial porosity (p_0), normal stress (P_n), box size (L, H) and specimen gradation (D_{max}/D_{min}): (a) poorly graded specimen; (b) well-graded specimen

in the range of lower values of box height and higher values of normal stress. The amount of strength increase varies from 30% to 120% within the range of box lengths tested, and from 0 to 30% within the range of box heights tested.

The above effects of box length scale and height scale can be better reflected when they are correlated to the box aspect ratio (L/H), as shown in Figs 6 and 7. It is found that the aspect ratio is a critical 'shape' factor, which controls the mechanism responsible for the bulk shear strength and failure behaviour of the granular specimen. In Figs 6 and 7, the trends of peak stress ratio against the aspect ratio are clearly marked by two groups of arrows that suggest the variations of peak stress ratio against the box length scale and height scale, respectively. Evidently in all the cases, the peak stress ratio decreases with increasing aspect ratio in both directions but a higher rate of change is found in the direction of constant height scale and decreasing length scale. This observation suggests that the box length scale may play a more dominant role in controlling the macro- and micromechanical shear behaviour of granular specimen than the box height scale.

An apparent explanation for the above size scale effects is the initial specimen porosity, which has been shown before to increase with increasing box length scale and decreasing box height scale. However, such an explanation is far from sufficient and convincing because it does not provide any insight on the micromechanics of granular media associated with the failure, shear localisation and evolution of shear

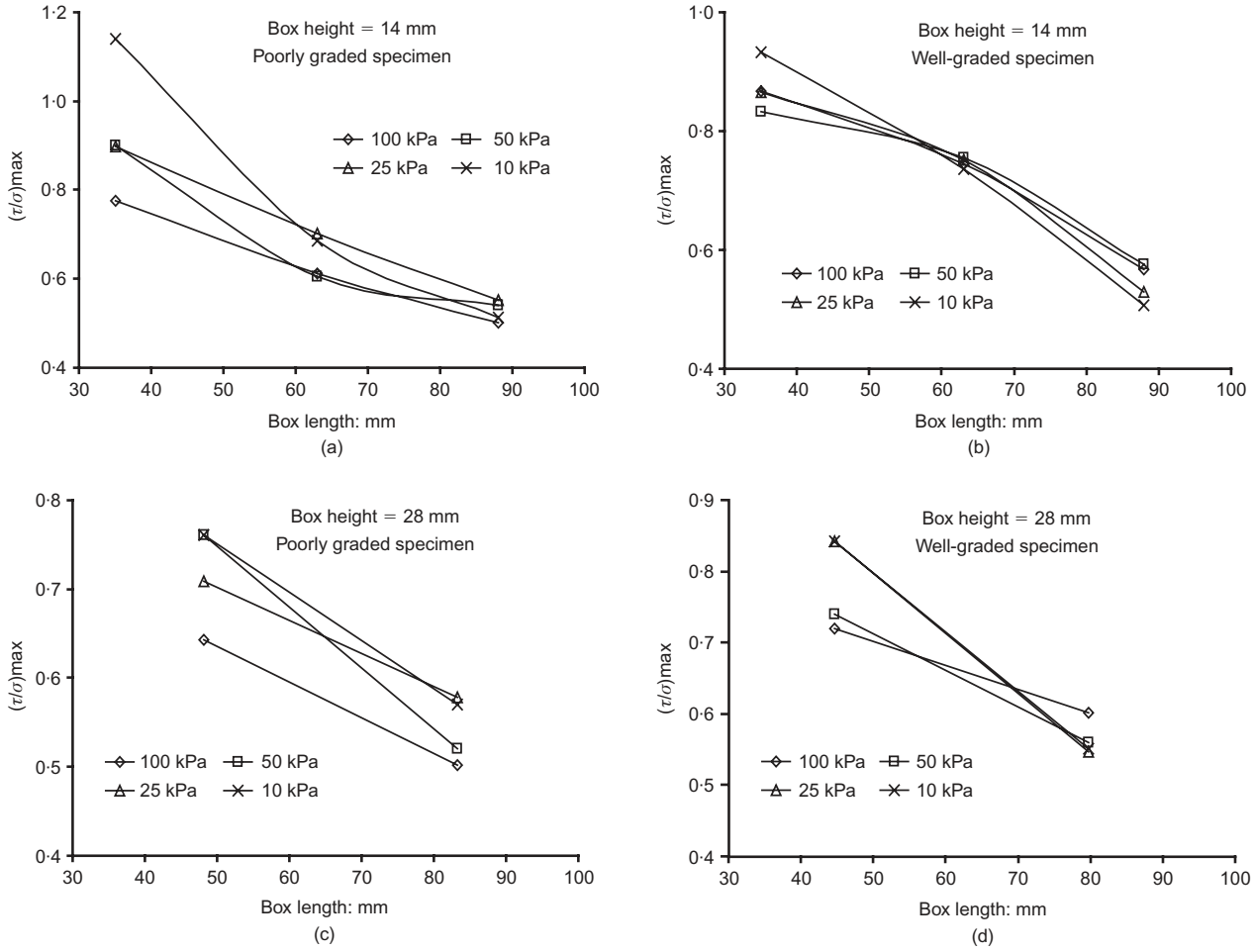

Fig. 4. Effects of the box length scale on the peak stress ratio

band under the influence of box size scale. Furthermore, the initial specimen porosity is itself a result of the box size scale, and therefore needs to be explained by micromechanics as well.

Micromechanical mechanisms and evidences

In order to reveal the mechanisms underlying the box size scale effect, the macroscopic simulation data need to be studied by a micromechanics-based analysis. As an example, in the following the micromechanical analysis on the data is made from two representative groups of simulations: one with L varying, $H = 14$ mm, $P_n = 100$ kPa and $D_{max}/D_{min} = 3{\cdot}0$, and the other with H varying, $L = 88$ mm, $P_n = 25$ kPa and $D_{max}/D_{min} = 3{\cdot}0$.

Effects of box length scale. The effects of varying box length (but with the other parameters fixed) on shear stress ratio and vertical displacement against shear displacement relations are shown in Figs 8(a) and 8(b). It can be seen that, although the peak stress ratio increases considerably when the box length decreases, the shear displacements corresponding to the peak stress ratios are close to each other. This means that similar magnitudes of boundary displacement are required fully to mobilise the material strength, although the amount of external work needed until the peak stress state increases with decreasing box length. In other words, the increase of box length scale (with respect to the particle size) has a slight influence on the extent of the granular portion which is influenced by the boundary movement and makes necessary changes of its local fabric to sustain the maximum stress until the peak stress state. The volume increase induced by the local fabric change is nearly proportional to the box length, as suggested by similar values of vertical displacement of the top wall incurred at each peak state (Fig. 8(b)). However, the highest rate of dilation at peak state is found in the 35 mm case, corresponding to the largest peak stress ratio, as expected.

In the following, the change in local fabric refers to the increase and rotation of shear-induced anisotropies in terms of contact normal and contact force orientation. Changes in these orientations are the main microscopic mechanism responsible for the development of bulk shear strength of granular material (Rothenburg, 1980; Bathurst & Rothenburg, 1990). The authors have previously quantified the shear strength between granular soils and solid rough surfaces in terms of shear-induced anisotropy (Wang *et al.*, 2007c, 2007d).

To better demonstrate the box length scale effect on the bulk shear behaviour, the shear stress ratio and volumetric strain are plotted against the applied shear strain, as shown in Figs 8(c) and 8(d). It is interesting to find that: (*a*) the shear strain at the peak stress ratio increases considerably when the box length scale decreases; (*b*) the volumetric strain increases in a much lower rate in the smaller length scale case; (*c*) the value of volumetric strain incurred at the peak states is almost independent of the length scale.

A reasonable explanation of the above observations is that the effects of progressive failure become more pronounced with the increase of box length scale. Progressive failure, as a keyword used in this paper, refers to the specific failure

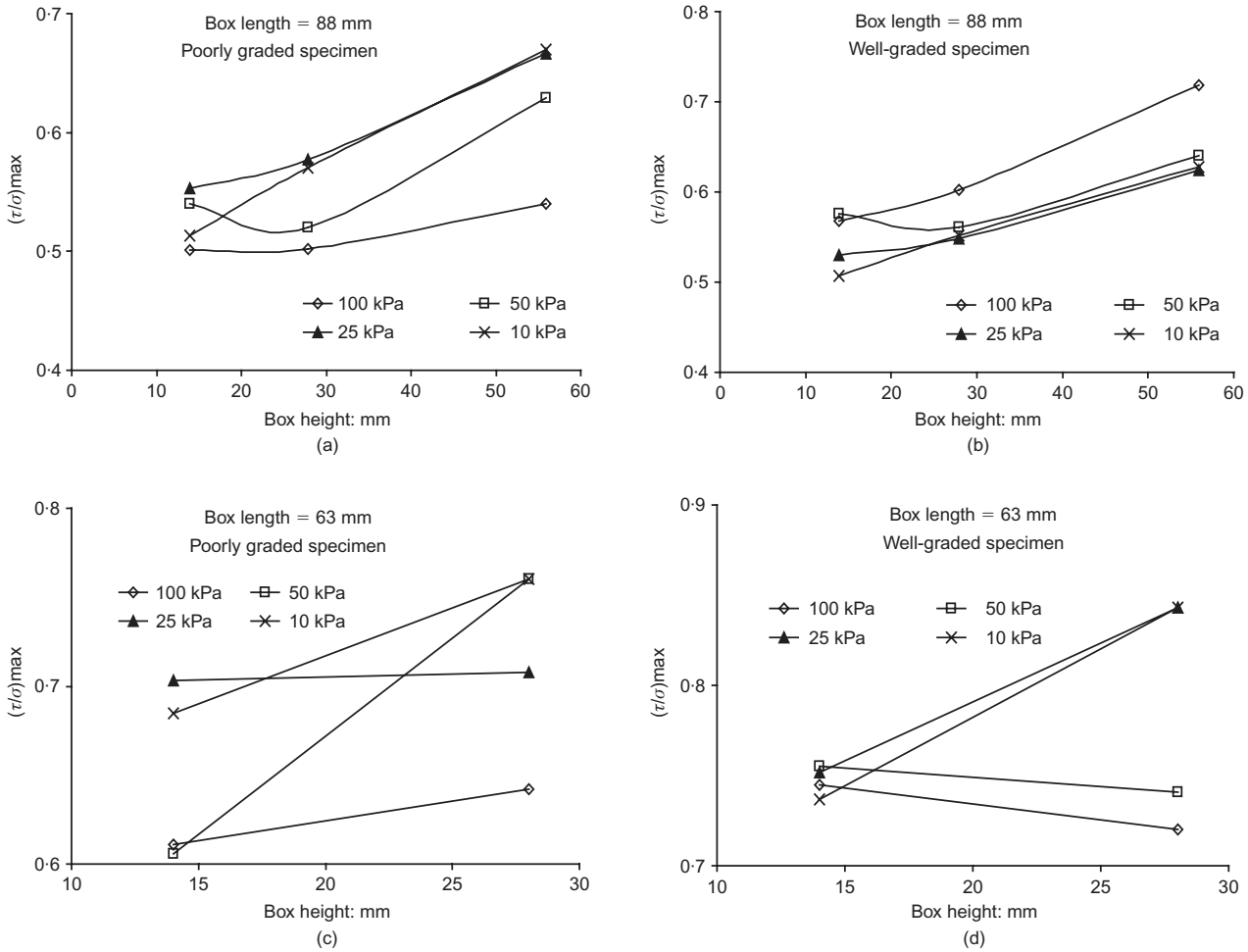

Fig. 5. Effects of the box height scale on the peak stress ratio

mode in which sequential failure of granular materials takes place as the boundary-induced shear localisation propagates from the lateral boundaries to the middle of the direct shear box. Apparently, for the large length scale ($L = 88$ mm for instance), the materials in the middle of the box length experience less shear straining than those closer to the lateral boundary in the small strain stage, meaning that the shear strength of the middle portion cannot be fully mobilised at the first peak stress state. It is observed that, for the $L = 88$ mm case, the stress and strain conditions in the middle of the box are quite uniform, with the pure shear mode dominating the material deformation during the pre-peak stage, as was previously reported by the authors (Wang *et al.*, 2007b).

Macroscopic evidence of progressive failure can also be observed in the stress ratio curves in Fig. 8(a). A few successive sub-peaks following the first peak in the $L = 88$ mm and 63 mm cases make the post-peak strain softening a longer process before the steady state is reached. In contrast, a sharp strain softening with much lower sub-peaks following a relatively broad peak plateau is observed in the 35 mm case. A more convincing example is given by the comparison between another pair of simulations with L varying, $H = 28$ mm, $P_n = 100$ kPa and $D_{max}/D_{min} = 1{\cdot}1$, as shown in Fig. 9. In this example, the 88 mm curve is characterised by two major peaks followed by a series of sub-peaks spanning a wide range of strain, and a lack of distinct post-peak strain softening stage. The continuing volume increase throughout the shearing process owing to the non-uniform fabric of the poorly graded material suggests that the well-defined steady state is never reached for both cases.

Microscopically, more insights could be gained when the contact force chains of the three simulations at their peak stress states are shown in Fig. 10. In this figure, the thickness of the line is proportional to the magnitude of the inter-particle contact force. It can be seen that the stress distribution is much more uniform in the larger length scale case than in the smaller length scale case. Furthermore, both the maximum and the average contact force magnitudes are much higher in the smaller length scale case, suggesting a higher mobilised material strength. In the 35 mm case, the larger contact force chains are more focused in the middle of the box, indicating that nearly the entire granular specimen is mobilised to resist the shear deformation (Fig. 10). In comparison, the contact forces in the other two cases are more uniformly distributed, especially in the middle of the box. This indicates that the current peak stress is attributable to the local material rearrangements closer to the boundaries bringing the materials to the verge of failure. The anisotropies of contact force distribution shown in Fig. 10 give further evidence of the above arguments. It is seen that both the magnitude and principal direction (θ) of the anisotropy decreases when the length scale increases, suggesting a higher degree of the material fabric has been mobilised in the smaller length scale case to sustain the external stress.

The effect of local/global failure at the peak stress state and the ensuing progressive failure as affected by the box length scale can be better visualised through the shear strain localisation which is calculated using the method previously developed by the authors (Wang *et al.*, 2007a, 2007b). Fig. 11 shows the shear strain distributions of the three simulations at their peak stress states. Clearly, a more pronounced

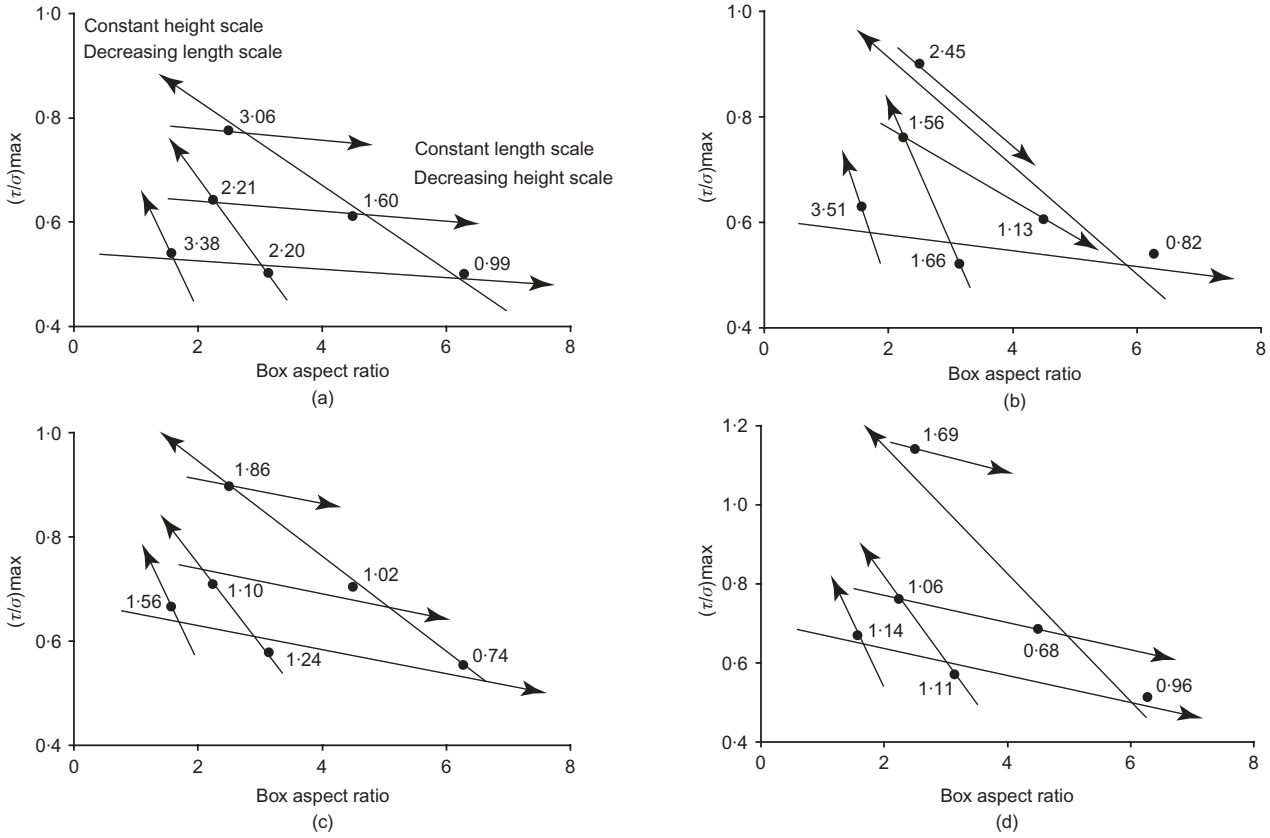

Fig. 6. Effects of the box aspect ratio (*L/H*) on the peak stress ratio for poorly graded specimens. Values besides the data points indicate the applied shear strains corresponding to their peak stress states: (a) normal stress = 100 kPa; (b) normal stress = 50 kPa; (c) normal stress = 25 kPa; (d) normal stress = 10 kPa

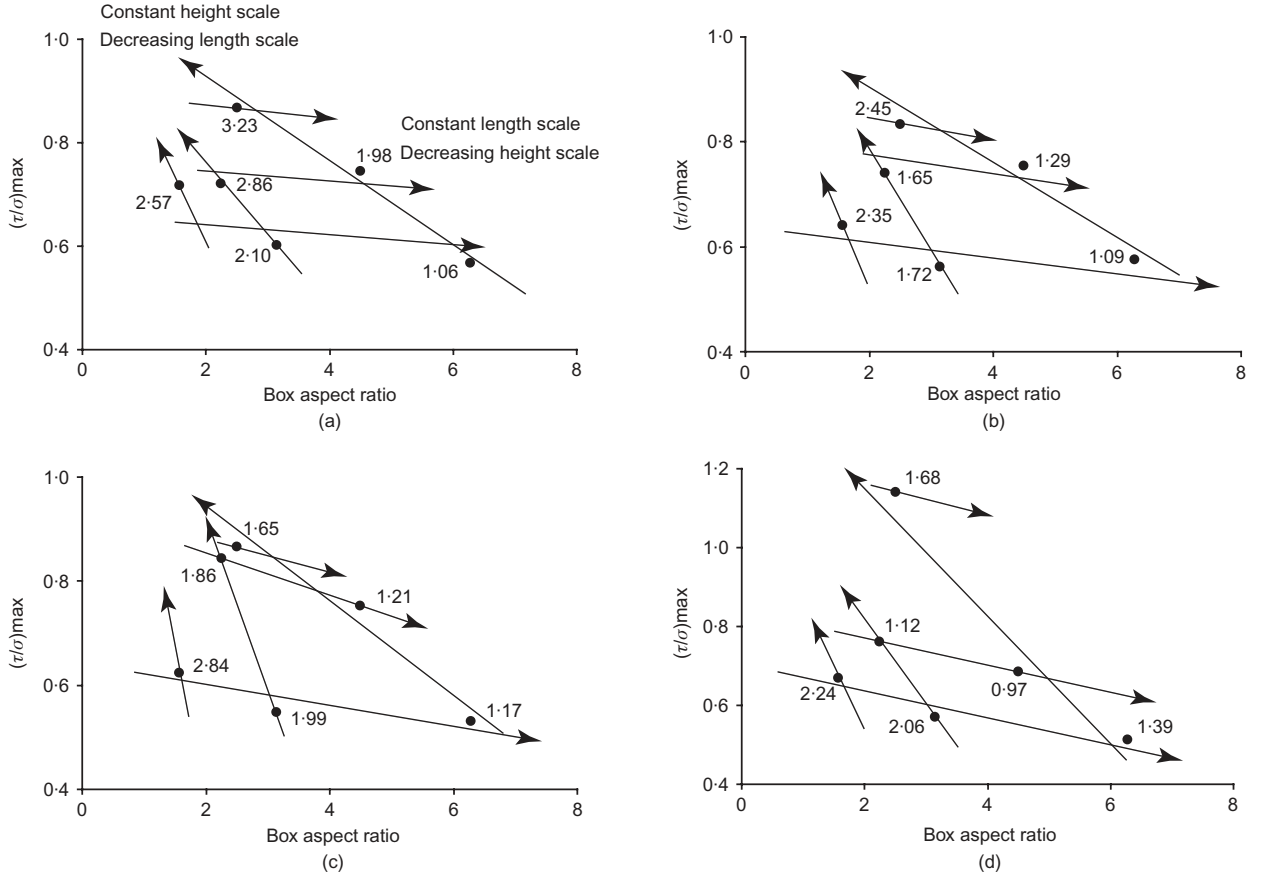

Fig. 7. Effects of the box aspect ratio (*L/H*) on the peak stress ratio for well-graded specimens. Values besides the data points indicate the applied shear strains corresponding to their peak stress states: (a) normal stress = 100 kPa; (b) normal stress = 50 kPa; (c) normal stress = 25 kPa; (d) normal stress = 10 kPa

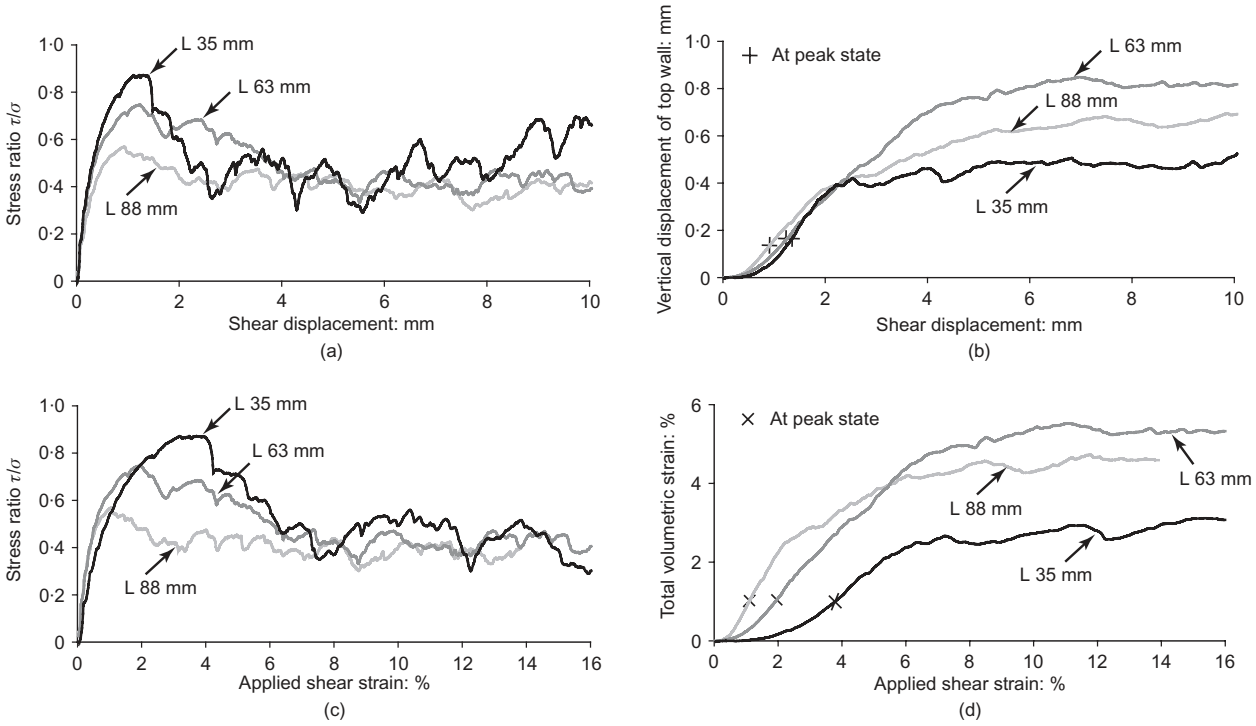

Fig. 8. Boundary-measured bulk simulation data from the first group of simulations with L varying, $H = 14$ mm, $P_n = 100$ kPa and $D_{max}/D_{min} = 3{\cdot}0$: (a) stress ratio ($\tau/\sigma$) against applied shear displacement; (b) vertical displacement of the top wall against applied shear displacement; (c) stress ratio (τ/σ)Δ vs. applied shear strain; (d) total volumetric strain against applied shear strain

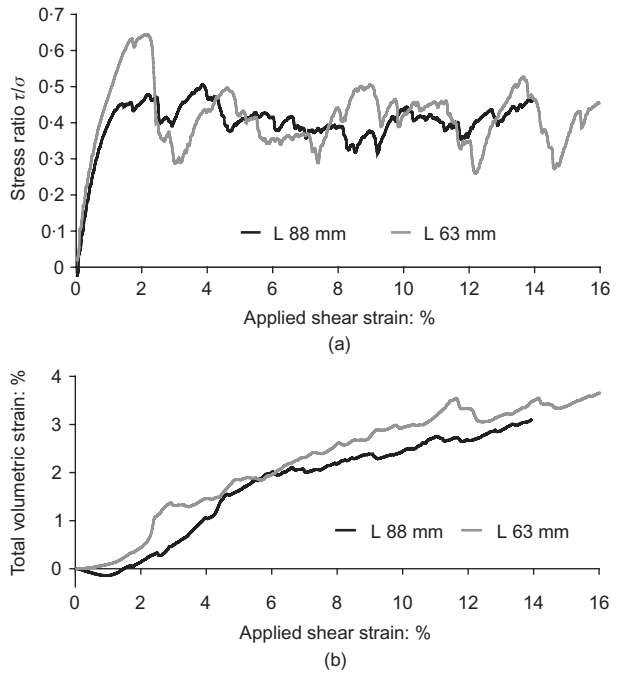

Fig. 9. Boundary-measured bulk simulation data for another pair of simulations with L varying, $H = 28$ mm, $P_n = 100$ kPa and $D_{max}/D_{min} = 1{\cdot}1$: (a) stress ratio ($\tau/\sigma$) against applied shear strain; (b) total volumetric strain against applied shear strain.

and concentrated shear band in the mid-plane of the box is found in the 35 mm case (Fig. 11(a)). In comparison, less developed shear bands deviating from the mid-planes of the box are found in the 63 mm and 88 mm cases (Figs 11(b) and 11(c)). In the latter two cases, rather than global and well-defined, shear bands are more local and less pronounced. Indeed, the bands are mainly composed of local structures subordinate to the primary structure of the shear band along the mid-plane during the subsequent shearing process (Scarpelli & Wood, 1982; Wang *et al.*, 2007a). As a comparison, the final structure of shear band at large shear strain is shown in Fig. 12. It can be seen that the difference between the structures of the shear bands at the two stages is least pronounced for the 35 mm case than the other two cases.

Effects of box height scale. A similar analysis performed on the data from the second group of simulations interestingly suggests that the same mechanism of global against progressive failure dominates the bulk strength behaviour of granular materials as the box height scale varies. In the following, the supporting macroscopic and microscopic evidences are briefly presented.

The stress ratio and vertical displacement against shear displacement relations, as well as the stress ratio and volumetric strain against applied shear strain relations are shown in Fig. 13. In this figure, the following consistent observations can be made

(*a*) the peak stress ratio increases when the box height increases, but the difference between the values for the 14 mm and 28 mm cases is much smaller
(*b*) the shear displacement (or shear strain) corresponding to the peak stress ratio increases considerably when the box height increases
(*c*) the absolute amounts of volume increase (dilation) indicated by the vertical displacements of the top wall at the peak stress states are similar for the 14 mm and 28 mm cases, and smaller than that of the 56 mm case
(*d*) the volumetric strain incurred at the peak stress ratio decreases considerably when the box height increases.

These observations indicate that a greater amount of external

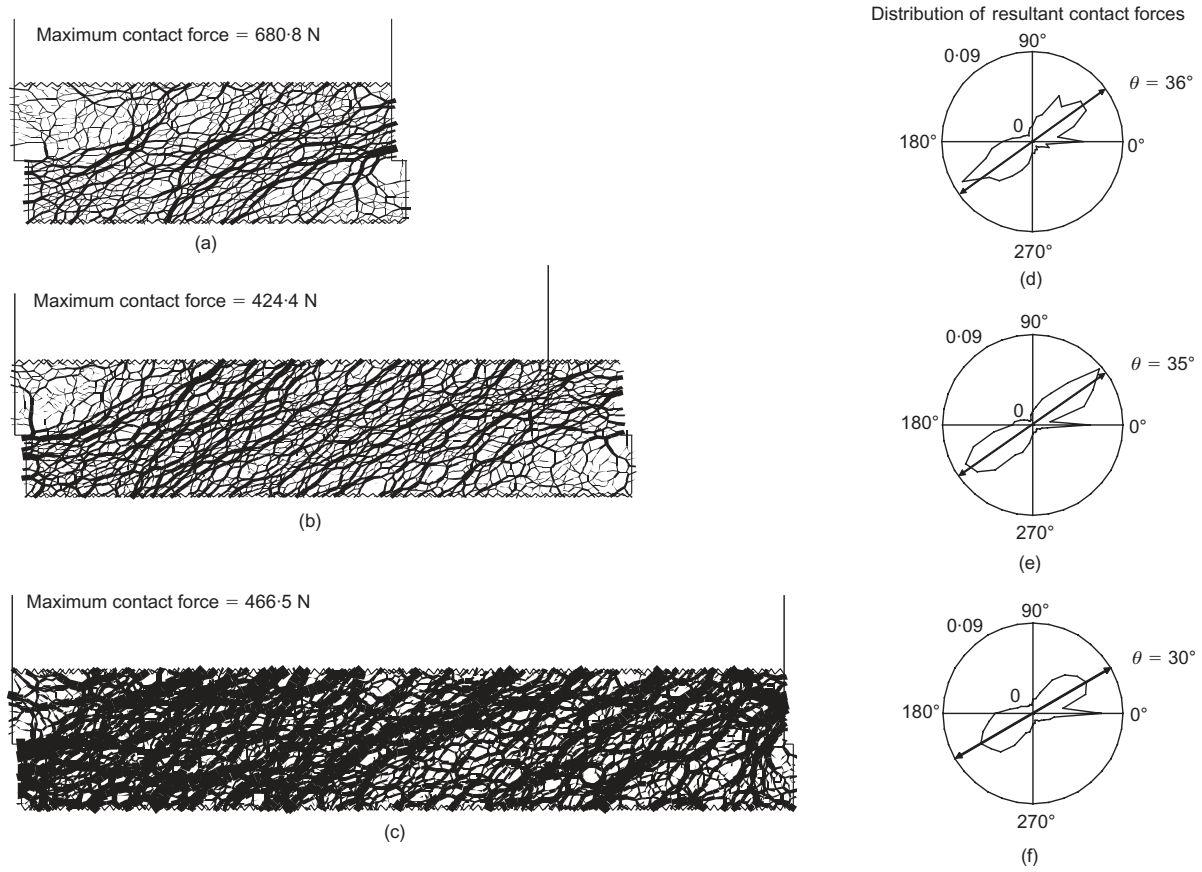

Fig. 10. Contact force networks and anisotropies inside the shear box of the first group of simulations captured at the peak stress state, (a)–(c) contact force network (with all the contact force lines in the three subplots scaled to the maximum contact force = 680·8 N in (a)): (a) $L = 35$ mm; (b) $L = 63$ mm; (c) $L = 88$ mm; (d)–(f) contact resultant force anisotropy: (d) $L = 35$ mm; (e) $L = 63$ mm; (f) $L = 88$ mm

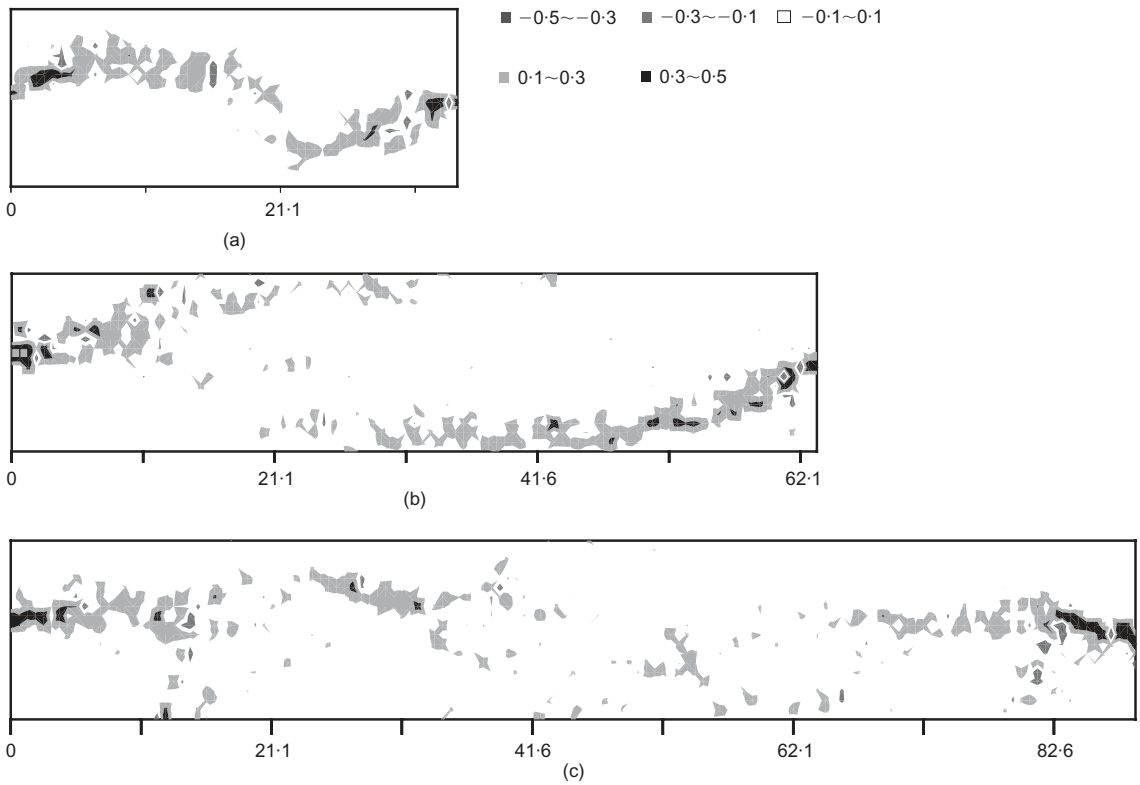

Fig. 11. Shear strain distributions inside the shear boxes of the first group of simulations captured at the peak stress state: (a) $L = 35$ mm; (b) $L = 63$ mm; (c) $L = 88$ mm

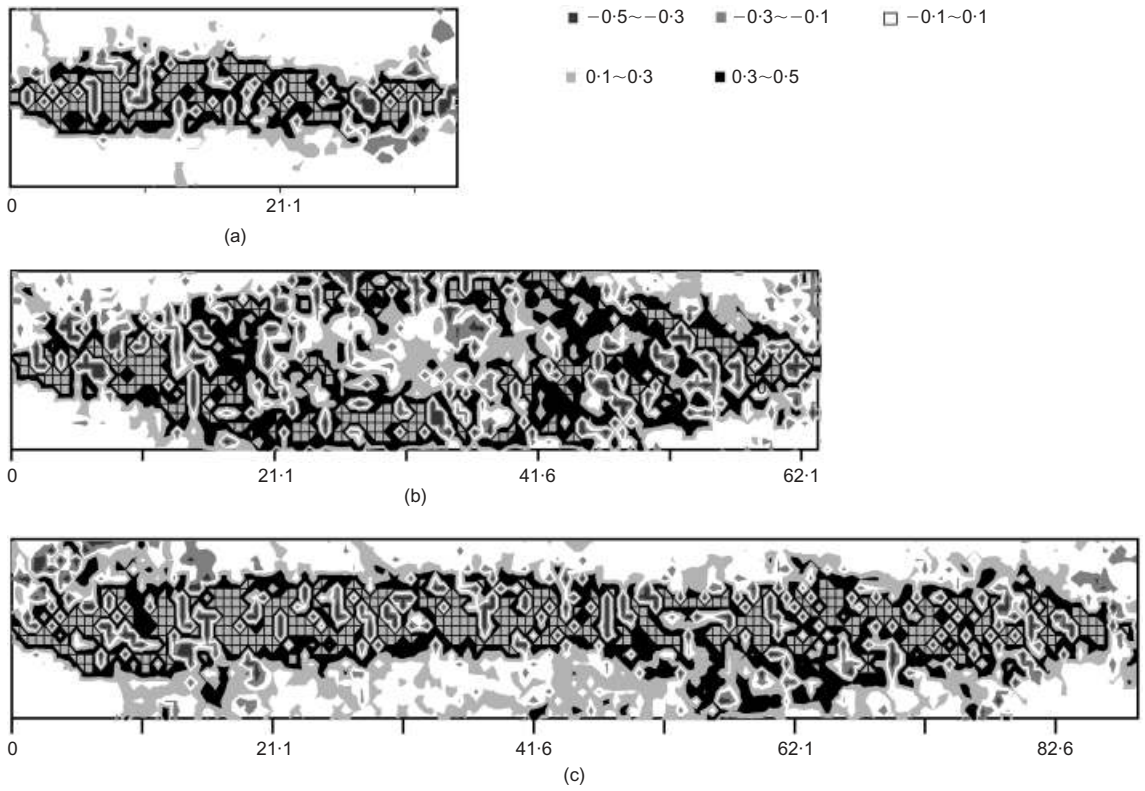

Fig. 12. Shear strain distributions inside the shear boxes of the first group of simulations captured at the steady state (12 mm shear displacement): (a) $L = 35$ mm; (b) $L = 63$ mm; (c) $L = 88$ mm

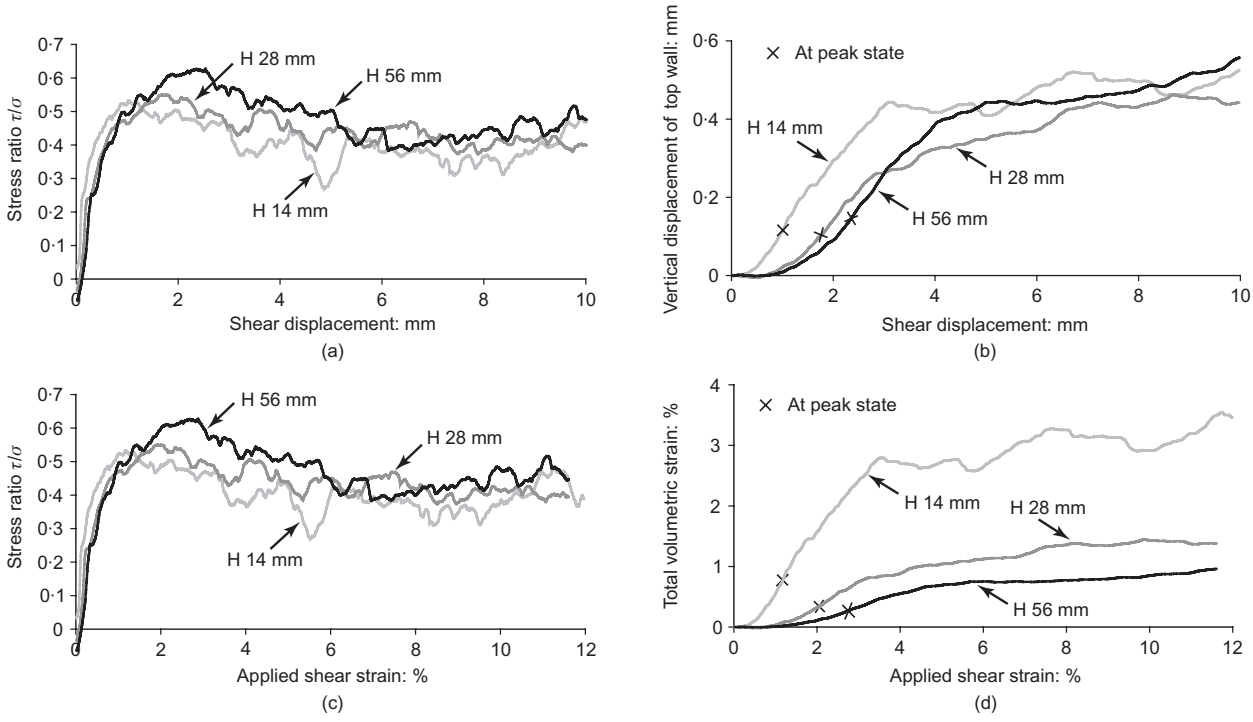

Fig. 13. Boundary-measured bulk simulation data from the second group of simulations with H varying, $L = 88$ mm, $P_n = 25$ kPa and $D_{max}/D_{min} = 3{\cdot}0$: (a) stress ratio $(\tau/\sigma)\Delta$ against applied shear displacement; (b) vertical displacement of the top wall against applied shear displacement; (c) stress ratio $(\tau/\sigma)\Delta$ against applied shear strain; (d) total volumetric strain against applied shear strain

work is exerted until the peak state to engage more granular material in the shearing when the box height scale is larger. In other words, progressive failure prevails in the cases with smaller box height scales.

Similarly, micromechanical evidence used to study the effects of box height includes the contact force chains and their anisotropies shown in Fig. 14, and the shear strain distributions shown in Fig. 15. At the peak stress state, the

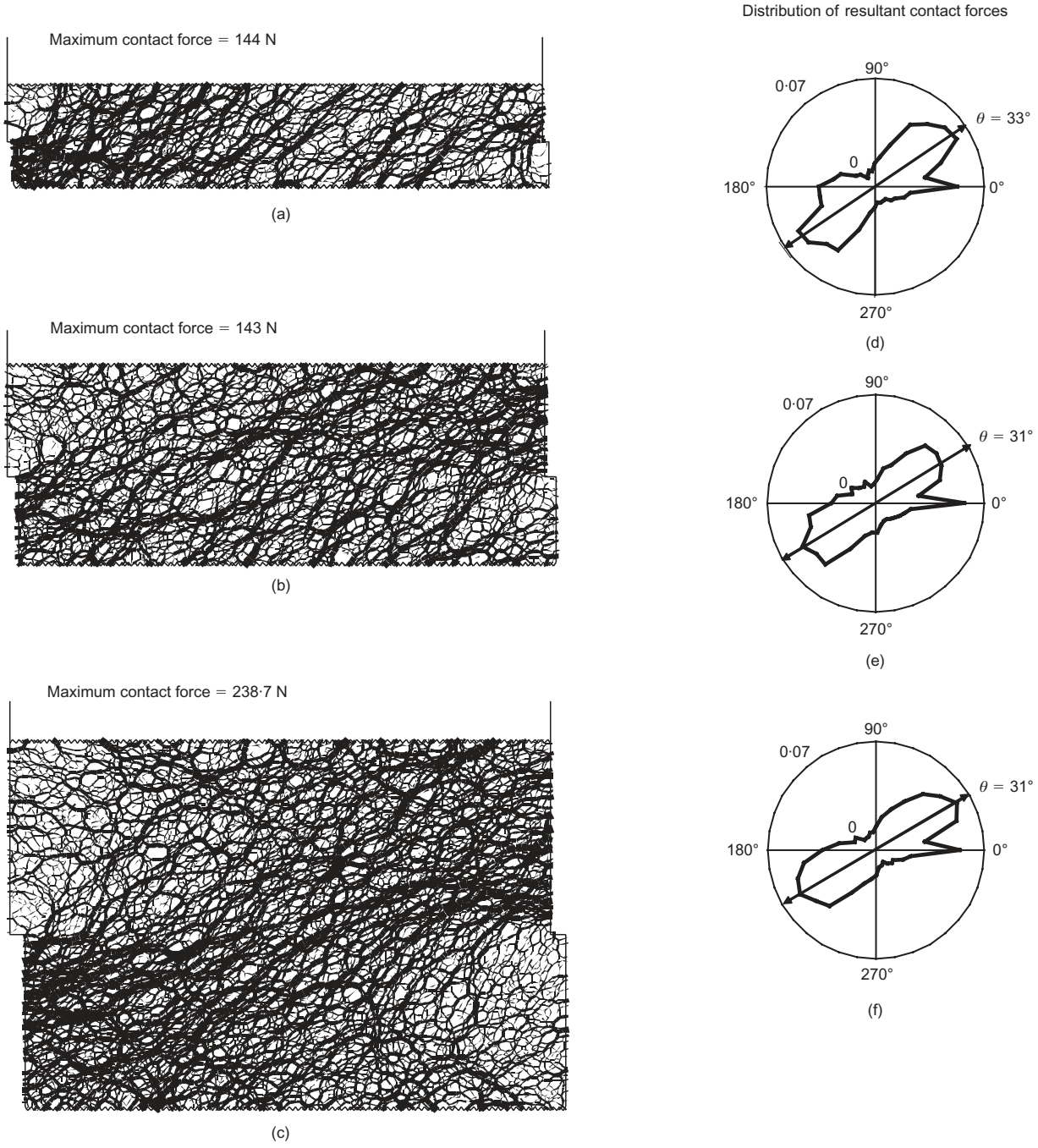

Fig. 14. Contact force networks and anisotropies inside the shear boxes of the second group of simulations captured at the peak stress state, (a)–(c) contact force network (with all the contact force lines in the three subplots scaled to the maximum contact force =238·7 N in (c)): (a) $H = 14$ mm; (b) $H = 28$ mm; (c) $H = 56$ mm; (d)–(f) contact resultant force anisotropy: (d) $H = 14$ mm; (e) $H = 28$ mm; (f) $H = 56$ mm

least uniform contact force distribution with the largest maximum/average contact force is found to occur in the 56 mm case, where the larger contact force chains are focused along the middle horizontal plane of the box (Fig. 14(c)). Correspondingly, a uniform and coherent shear band throughout the length of the box appears at the middle shear plane, suggesting a global failure of the specimen following the peak stress state (Fig. 15(c)). In the other two cases, the contact force distribution is more uniform, and the maximum/average contact force is also much lower. Partial stress concentrations occur near both ends of the box (Figs 14(a) and 14(b)). Shear bands appear in a more dispersed manner. Smaller-scale shear bands deviating from the middle shear plane prevail at the peak stress state, especially in the 28 mm case, suggesting the bulk peak strength is being controlled by the local failure near the boundaries (Fig. 15(b)). The arguments become more convincing when the final shear bands are shown in Fig. 16. Interestingly, the extents of the final shear bands are similar for the three cases, but the one in the 14 mm case is artificially limited by the upper and lower boundaries owing to the insufficient height of the specimen (Fig. 14(a)).

CONCLUDING REMARKS

It has been shown that for both direct shear box length and height size scales, the major mechanism governing the observed bulk strength behaviour is controlled by the local against global fabric change, strain localisation and shear band failure as a function of the imposed boundary con-

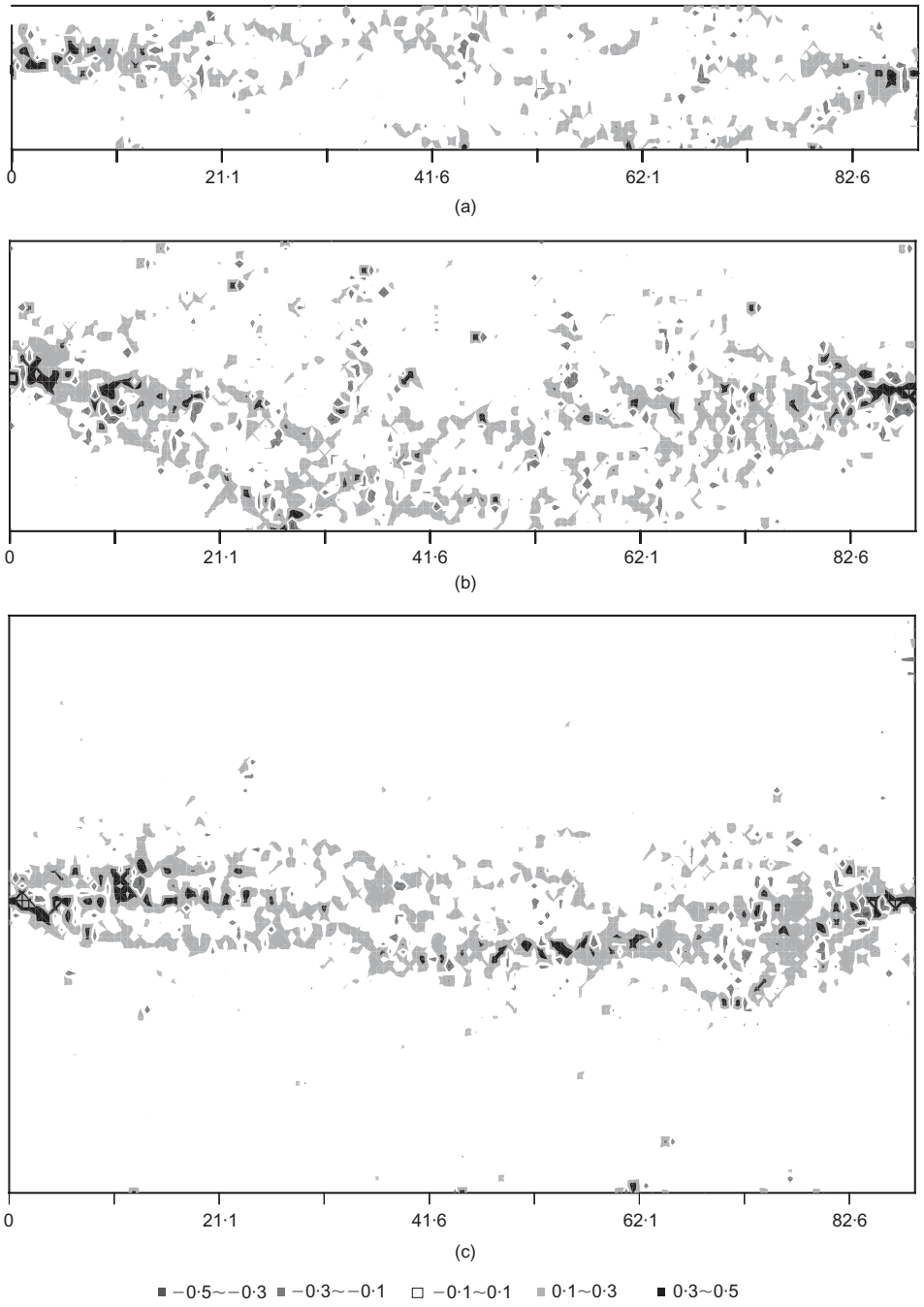

Fig. 15. Shear strain distributions inside the shear boxes of the second group of simulations captured at the peak stress state: (a) $H = 14$ mm; (b) $H = 28$ mm; (c) $H = 56$ mm

straint. Progressive failure, which occurs when the boundary-induced shear localisation propagates from the lateral boundaries towards the middle of the box, is the main feature of the behaviour adopted by the granular material in response to the imposed external shear strain. It was found that the effects of the box length and height scales can be correlated by their connecting bridge; that is, the box aspect ratio *L/H*. It is found that in both cases, progressive failure becomes more likely when *L/H* becomes larger. Equivalently, global failure tends to control the bulk strength behaviour when *L/H* is smaller.

It has been shown in Figs 6 and 7 that the peak stress ratio decreases with the increasing *L/H*, when either *L* or *H* is fixed. However, more evidence of the aspect ratio effects can be shown. The numbers beside each data point in Figs 6 and 7 indicate the applied shear strains at each corresponding peak stress state. It can be seen that this value increases with decreasing *L/H* when either *L* or *H* is fixed. This observation implies that the aspect ratio is a critical 'shape' factor that controls the direct shear behaviour of granular materials. When *L/H* is small, the long-range contact force chains stemming from the lateral boundaries could extend farther into the inner part of the specimen and avoid the interference from the top and bottom boundaries. As a result, global failure involving the entire specimen is a more probable result. However, when *L/H* is large, the contact force chains are quickly interfered by the upper and lower boundaries, and therefore cannot extend far into the inner specimen. Consequently, local failure and shear bands inclined from the middle shear plane form.

From the above discussion, it is concluded that a larger direct shear box with a smaller *L*/*H* aspect ratio is favoured for yielding more correct bulk direct shear strength para-

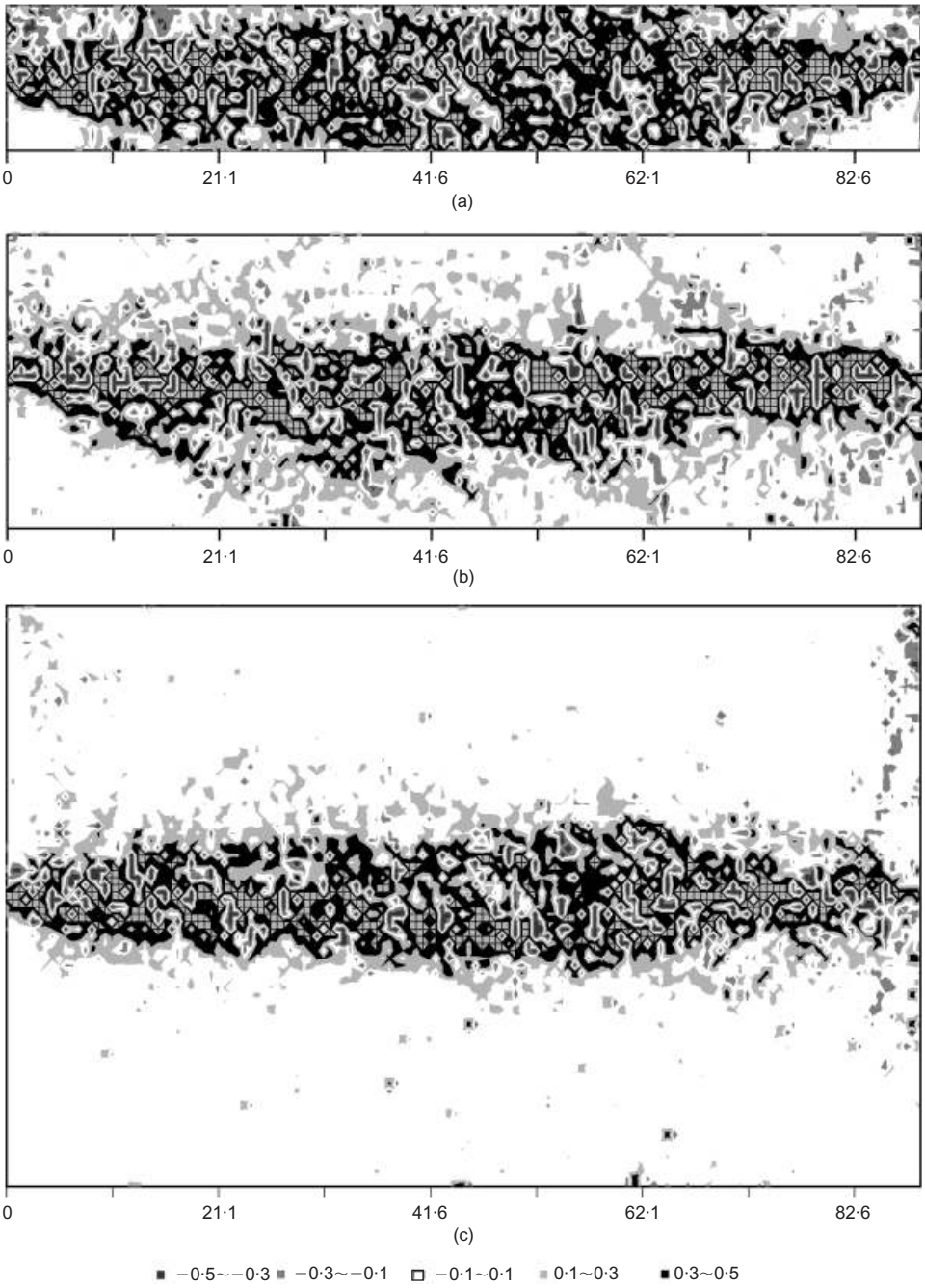

Fig. 16. Shear strain distributions inside the shear boxes of the second group of simulations captured at the steady state (12 mm shear displacement): (a) $H = 14$ mm; (b) $H = 28$ mm; (c) $H = 56$ mm

meters for granular soils because it gives a more global and uniform failure of the entire specimen. Based on the range of box size scale tested in the current study, it is recommended that a minimum value of 60 for L/D_{max}, a minimum value of 40 for H/D_{max} and a range of 1·5 to 2 for L/H should be used as optimal for direct shear testing. These values represent the minimum threshold where the box scale effects (i.e. local and progressive failure) disappear. However, discretion should be exercised to select an appropriate shear device that best simulates the boundary conditions in the field. Very often, progressive failure is exactly the in situ failure mode governing the performance of geotechnical systems. Theoretically, further quantifications of the specimen scale effects on the macroscopic behaviour of granular materials will rely on the fundamental understanding of quantitative relationships between material fabric, anisotropy and bulk strength.

ACKNOWLEDGEMENTS

The study presented in this article was supported by The Petroleum Research Fund, American Chemical Society under grant No. ACS PRF# 43848-AC8, and Start-up Fund of City University of Hong Kong under grant No. 7200132. This support is gratefully acknowledged.

REFERENCES

Alshibli, K. A. & Sture, S. (2000). Shear band formation in plane strain experiments of sand. *J. Geotech. Geoenviron. Engng* **126**, No. 6, 495–503.

ASTM (American Society for Testing and Materials) (2002). *Standard test method for determining the coefficient of soil and geosynthetic or geosynthetic and geosynthetic friction by the*

direct shear method, D5321-02. West Conshohocken, PA: ASTM.

ASTM (American Society for Testing and Materials) (1990). *Standard test method for direct shear tests of soils under consolidated drained conditions*, D3080-90. West Conshohocken, PA: ASTM.

Arthur, J. R. F., Dunstan, T., Al-Ani, G. A. J. L. & Assadi, A. (1977). Plastic deformation and failure in granular media. *Géotechnique* **27**, No. 1, 53–74, **doi**: 10.1680/geot.1977.27.1.53.

Bathurst, R. J. & Rothenburg, L. (1990). Observation on stress–force–fabric relationships in idealized granular materials. *Mech. Mater.* **9**, 65–80.

Cerato, A. B. & Lutenegger, A. L. (2006). Specimen size and scale effects of direct shear box tests of sands. *Geotech. Testing J.* **29**, No. 6, 1–10.

Dove, J. E. (1996). *Particle–geomembrane interface behavior as influenced by surface topography.* PhD thesis, Georgia Institute of Technology, Atlanta, Georgia, USA.

Dove, J. E., Bents, D. D., Wang, J. & Gao, B. (2006). Particle-scale surface interactions of non-dilative interface systems. *Geotextiles Geomembranes* **24**, No. 3, 156–168.

Dove, J. E. & Jarrett, J. B. (2002). Behavior of dilative sand interface in a geotribology framework. *J. Geotech. Geoenviron. Engng* **128**, No. 1, 25–37.

Hartl, J. & Ooi, J. Y. (2008). Experiments and simulations of direct shear tests: porosity, contact friction and bulk friction. *Granular Matter* **10**, No. 4, 263–271.

Hvorslev, M. J. (1960). Physical components of the shear strength of saturated clays. *Proceedings of the research conference on shear strength of cohesive soils*, Boulder, pp. 437–501.

IChemE (1989). *Standard shear test technique for particulate solids using the Jenike shear cell*. Institution of Chemical Engineers, London.

Itasca Consulting Group, Inc. (2002). *PFC2D – Particle flow code in 2 dimensions, version 3.0*. Itasca Consulting Group, Inc., Minneapolis, MN, USA.

Jacobson, D. E., Valdes, J. R. & Evans, T. M. (2007). A numerical view into direct shear specimen size effects. *Geotech. Testing J* **30**, No. 6, 512–516.

Jewell, R. A. & Wroth, C. P. (1987). Direct shear tests on reinforced sand. *Géotechnique* **37**, No. 1, 53–68, **doi**: 10.1680.geot.1987.37.1.53.

Lings, M. L. & Dietz, M. S. (2004). An improved direct shear apparatus for sand. *Géotechnique* **54**, No. 4, 245–256, **doi**: 10.1680/geot.2004.54.4.245.

Morgenstern, N. R. & Tchalenko, J. S. (1967). Microscopic structure in kaolin subjected to direct shear. *Géotechnique* **17**, No. 4, 309–328, **doi**: 10.1680/geot.1967.17.4.309.

Palmeira, E. M. & Milligan, G. W. E. (1989). Scale effects in direct shear tests on sand. *Proc. 12th Int. Conf. Soil Mech. Found. Engng, Rio de Janeiro, Brasil* **1**, 739–742.

Parsons, J. D. (1936). Progress report on an investigation of the shearing resistance of cohesionless soils. *Proc. 1st Int. Conf. on Soil Mech. Found. Engng, Cambridge, Massachusetts* **2**, 133–138.

Potts, D. M., Dounias, G. T. & Vaughan, P. R. (1987). Finite element analysis of the direct shear box test. *Géotechnique* **37**, No. 1, 11–23, **doi**: 10.1680/geot.1987.37.1.11.

Rothenburg, L. (1980). *Micromechanics of idealized granular system*. PhD thesis, Carleton University, Ottawa, Ontario, Canada.

Saada, A. S. & Townsend, F. C. (1981). State of the art: laboratory strength testing of soils. *Laboratory shear strength of soils, ASTM Spec. Tech. Publ.* **740**, 7–77.

Scarpelli, G. & Wood, D. M. (1982). Experimental observations of shear band patterns in direct shear tests. *Proceedings of the IUTAM conference on deformation and failure of granular materials*, Delft, pp. 472–484.

Terzaghi, K. & Peck, R. B. (1948). *Soil mechanics in engineering practice*. New York: Wiley.

Vucetic, M. & Lacasse, S. (1982). Specimen size effect in simple shear test. *J. Geotech. Engng Div. ASCE* **108**, No. 12, 1567–1585.

Wang, J. (2006). *Micromechanics of granular media: a fundamental study of interphase systems*. PhD thesis, Virginia Tech, Blacksburg, Virginia, USA.

Wang, J. & Gutierrez, M. S. (2009). Modeling of scale effects on the micromechanics of granular media under direct shear condition. *Powders and Grains 2009, Golden, Colorado* **1145**, 365–368.

Wang, J., Gutierrez, M. S. & Dove, J. E. (2004). Effects of particle rolling resistance on interface shear behavior. *Proc. 17th Conf. Engng Mech., Newark* **65**, 56–63.

Wang, J., Gutierrez, M. S. & Dove, J. E. (2007a). Numerical studies of shear banding in interface shear tests using a new strain calculation method. *Int. J. Numer. Analytical Methods in Geomech*. **31**, No. 12,1349–1366.

Wang, J., Dove, J. E. & Gutierrez, M. S. (2007b). Discrete-continuum analysis of shear band in the direct shear test. *Géotechnique* **57**, No. 6, 513–526, **doi**: 10.1680/geot.2007.57.6.513.

Wang, J., Dove, J. E. & Gutierrez, M. S. (2007c). Determining particulate–solid interphase strength using shear-induced anisotropy. *Granular Matter* **9**, Nos 3–4, 231–240.

Wang, J., Dove, J. E. & Gutierrez, M. S. (2007d). Anisotropy-based failure criterion for an interphase system. *J. Geotech. Geoenviron. Engng, ASCE* **133**, No. 5, 599–608.

Zhang, L. & Thornton, C. (2007). A numerical examination of the direct shear test. *Géotechnique* **57**, No. 4, 343–354, **doi**: 10.1680/geot.2007.57.4.343.